Applied Catalysis A: General 517 (2016) 110–119

Contents lists available at ScienceDirect

Applied Catalysis A: General

journal homepage: www.elsevier.com/locate/apcata

Heterogeneous hydrogenation of nitroaromatic compounds on gold catalysts: Influence of titanium substitution in MCM-41 mesoporous supports

Cecilia C. Torres[a,*], Joel B. Alderete[a], Gina Pecchi[b], Cristian H. Campos[b], Patricio Reyes[b], Bárbara Pawelec[c], Eliana G. Vaschetto[d], Griselda A. Eimer[d]

[a] Departamento de Química Orgánica, Facultad de Ciencias Químicas, Universidad de Concepción, Edmundo Larenas 129, Casilla 160-C, Concepción, Chile
[b] Departamento de Fisicoquímica, Facultad de Ciencias Químicas, Universidad de Concepción, Edmundo Larenas 129, Casilla 160-C, Concepción, Chile
[c] Instituto de Catálisis y Petroleoquímica (ICP-CSIC), Grupo de Energía y Química Sostenible (EQS), c/Marie Curie s/n Cantoblanco, Madrid, Spain, Spain
[d] Centro de Investigación y Tecnología Química (CITeQ), Universidad Tecnológica Nacional, Facultad Regional Córdoba, Maestro López esq. Cruz Roja Argentina, 5016, C. Universitaria, Córdoba, Argentina

ARTICLE INFO

Article history:
Received 1 September 2015
Received in revised form 10 February 2016
Accepted 10 February 2016
Available online 16 March 2016

Keywords:
Ti-MCM-41 supports
Gold catalyst
Nitrobenzene-compounds hydrogenation
QSPR

ABSTRACT

A series of Ti-modified MCM-41 supports and their respective Au catalysts were prepared and characterized to study the effect of titanium into the support and on the characteristics of the Au surface species for heterogeneous hydrogenation of aromatic nitrocompounds. The systems were characterized by X-ray diffraction, Infrared spectroscopy (FT-IR), transmission electron microscopy (TEM), diffuse reflectance UV–vis (DRUV–vis), N_2 adsorption–desorption isotherms, ICP-MS and X-ray photoelectron spectroscopy (XPS). Additionally, these catalysts were tested for the hydrogenation of nitrobenzene in a batch-type reactor using ethanol as the solvent at 25 °C. Based on a combined FT-IR and DRUV–vis was possible to conclude that the Ti(IV) is incorporated into the framework of MCM-41 and Ti-containing MCM-41 catalysts were more active than an MCM-41 unmodified catalyst. The Ti(X)-MCM-41 supports prepared with Ti 2.0 wt% incorporation showed the best catalytic performance, which was attributed to an optimal number of isolated Ti sites that increased the Au stability on the support surface. For this system, the effect of the H_2 pressure, solvent nature and recyclability of the catalyst was also studied. Finally, a quantitative structure property relationship (QSPR) model was obtained for the catalytic activities of *para*-substituted nitrobenzenes. The multilinear model considered two parametric descriptors: the sigma constant (σ) and the hydrophobic π-constant, which account for the electronic and hydrophobic effect of the substituents.

1. Introduction

Inorganic materials with controlled pore size distribution are very interesting because of the wide number of applications in which they are used [1]. In 1992, Mobil Corporation [2] reported a novel concept in the synthesis of molecular sieves that used the advantageous properties of surfactant molecules to self-assemble and form liquid crystal-type structures, creating a new family of mesoporous molecular sieves called M41S [3,4]. These types of solids have pore diameters ranging from 2 to 10 nm, a mesoporous volume ranging from 0.7 to 1.2 $cm^3\ g^{-1}$ [5] and large and accessible internal areas (higher than 1000 $m^2\ g^{-1}$). The most important and used mesoporous molecular sieve is MCM-41 because of its hexagonal arrangement of uniformly sized mono-dimensional pores and its reliable synthesis [6–9]. Thus, pure silica MCM-41, heteroatom-doped MCM-41, and functionalized MCM-41 materials have been widely investigated because they have important applications in catalysis, separation, and nano-engineering fields [10–16].

On the other hand, gold nanoparticles (Au NPs) supported on mesoporous oxides are widely employed as heterogeneous catalysts for fine chemical production [17,18]. It is well established that the catalytic activity of supported gold nanoparticles depends on the particle size and the nature of the support [19–21]. Among the reactions studied, the hydrogenation of nitroaromatic derivatives is important because the aromatic amines are intermediates in the production of a range of pharmaceuticals, agrochemicals, cosmetics, herbicides, dyes and polymers [22,23]. Moreover, hydrogenation using molecular hydrogen is non-polluting and is

* Corresponding author.
E-mail address: cectorres@udec.cl (C.C. Torres).

http://dx.doi.org/10.1016/j.apcata.2016.02.013
0926-860X/

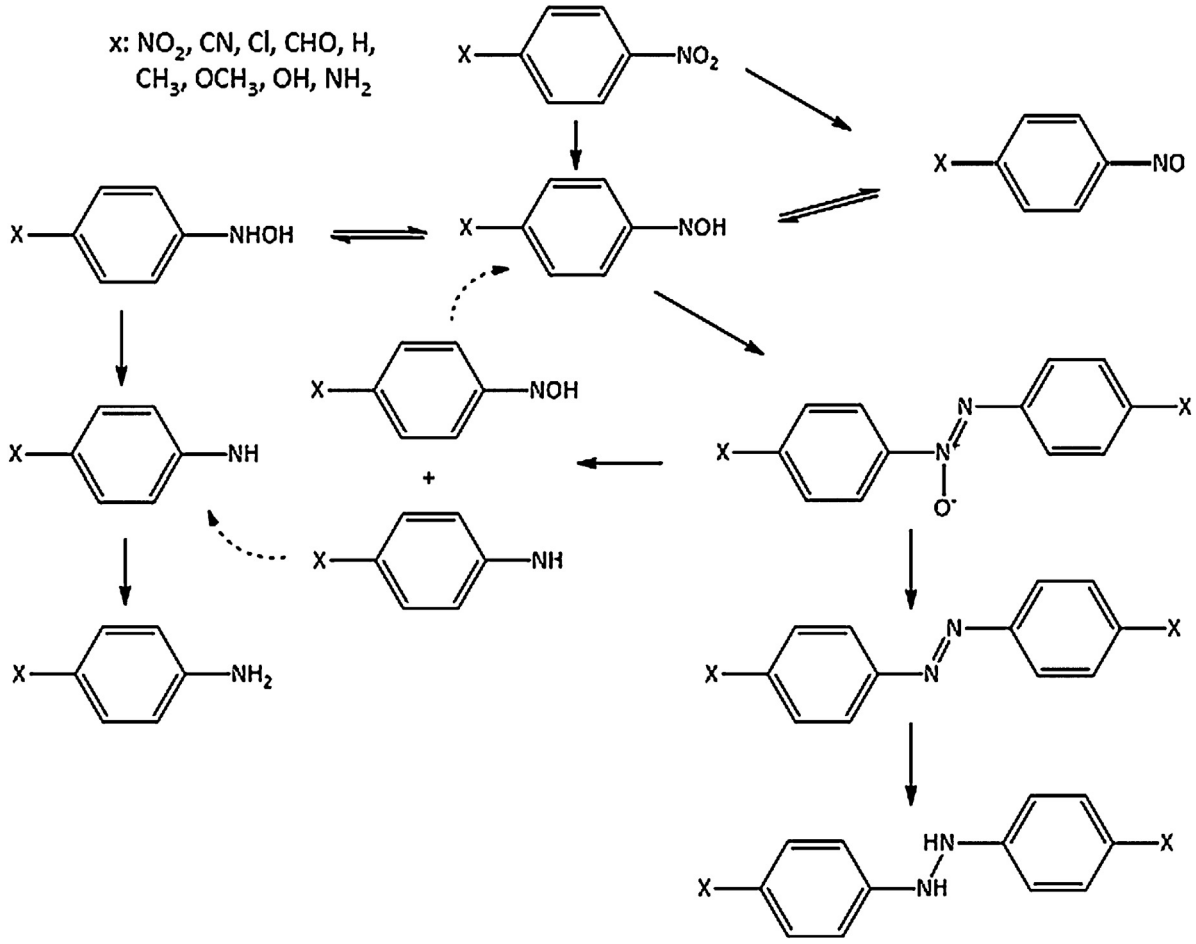

Scheme 1. Reaction pathways for *para*-substituted nitrobenzene hydrogenation (hydrogen and water are not depicted) adapted from Ref. [59].

considered an ecofriendly alternative to the commonly used reduction reactions to obtain the desired aromatic amines.

The use of Au as an active phase requires the development of newer and novel catalysts in order to achieve higher catalytic activity and selectivity under mild or ambient reaction conditions. Many studies have been attempted on supported Au in order to achieve a high catalytic performance using supports in the form of nanocomposites in which gold nanoparticles are loaded onto support materials such as molecular sieves, metal oxides, polymers and activated carbon [18,20,24,25].

In this paper, a series of titanium-containing mesoporous molecular sieves with a Ti wt% from 0 to 10.7 were prepared by hydrothermal synthesis. These materials were used as a support for Au NPs to obtain metallic catalysts at 1 wt% on the Ti(X)MCM-41. The application of an MCM-41 molecular sieve as a support for Au NPs is limited to some extent because of a lack of active sites in the neutral purely siliceous framework during the Au deposition [17,26]. The incorporation of heteroatoms as extra-framework nanoscale oxide clusters or in an appropriate valence state as a tetrahedral framework species might generate preferential sites for the deposition of the metal clusters. Ti is one of the most attractive heteroatoms introduced into mesoporous molecular sieves due to suitable acid/redox properties and good enough stabilization of Au NPs, as was previously reported for Au/TiO_2 catalysts [21].

The hydrogenation of nitrobenzene (NB) was chosen as the test reaction in semi-batch conditions for the Ti(X)MCM-41 systems to evaluate the activity and selectivity of the catalysts at different nominal Ti substitutions on the surface of the supports. For the best Au/Ti(X)-MCM-41 systems, reaction parameters such as the H_2 pressure, solvent nature, and recyclability were investigated in

Table 1
Chemical composition and surface properties of Ti(X)-MCM-41 supports.

Support Ti(X)-MCM-41	Ti (%wt)	ZPC[a] pH	S_{BET}[b] (m^2g^{-1})	Pore[c] (nm)	V_T[d] (cc/g)	d_{100}[e] (nm)	a_0[f] (Å)
0	–	1.5	1035	3.7	0.98	3.882	44.9
1.0	0.9	2.0	1000	2.6	0.57	3.623	41.8
2.0	2.0	2.4	979	2.9	0.43	3.610	41.7
5.4	5.3	2.8	864	4.7	0.31	3.594	41.2
10.7	9.3	3.2	786	3.6	0.40	3.516	40.5

[a] Determined from ZPC vs pH measurement.
[b] Specific area calculated from BET method.
[c] Determined from BJH method.
[d] Pore volume determined at $P/P^{\circ} = 0.99$.
[e] determined by XRD.
[f] $a_o = 2d_{100}/\sqrt{3}$.

detail to optimize the selectivity and catalytic performance of the catalyst. Finally, the optimized Au/Ti(x)-MCM-41 catalyst was used in the liquid phase hydrogenation of a series of *para*-substituted nitroaromatic compounds, and the catalytic data were analyzed in a Quantitative Structure Property Relationship (QSPR) study.

2. Experimental

2.1. Preparation of the supports

The MCM-41 support was prepared by the reaction of an aqueous solution of tetramethylammonium hydroxide (TMAOH) and cetyltrimethylammonium bromide (CTMABr) with aerosil silica with continuous stirring as in the standard procedure [5,27]. The resulting homogeneous gel (pH 11) had a molar composition of SiO_2:0.15CTMABr:0.26 TMAOH: 24.3 H_2O and was dried and calcined for 1 h in flowing N_2, followed by 12 h in a dynamic air flux at 500 °C for both calcinations.

The titanium-containing mesoporous materials with various Ti substitution contents were synthesized as reported previously [28,29]. Briefly, CTABr was dissolved in water and a 2.0 mol L^{-1} NaOH aqueous solution. After heating slightly (35–40 °C) to dissolve the surfactant, tetraethoxysilane (TEOS) was added. After 30 min, titanium butoxide was incorporated into the mixture. The mol ratios of the reactants were as follows: NaOH/Si = 0.50, CTABr/Si = 0.12, H_2O/Si = 132 and Si/Ti = 10, 20, 60, 120 to obtain nominal Ti loadings of 1.0, 2.0, 5.4 and 10.7 wt%, respectively. The resultant mixture was stirred at room temperature for 4 h. Then, this gel was heated at 70 °C with stirring in a closed propylene flask. The final solid was filtered, washed with distilled water until pH 7 was achieved and dried at 60 °C overnight. To remove the template, the samples were heated (heating rate of 2 °C/min) under a N_2 (60 mL/min) flow up to 500 °C, maintaining this temperature for 6 h, and then subsequently calcined at 500 °C under an air flow for 6 h. All of the supports are denoted by Ti(x)-MCM-41, where the "X" corresponds to the Ti nominal wt%.

2.2. Catalyst preparation

The Au/Ti(X)MCM-41 catalysts were prepared by a homogeneous deposition–precipitation method using NaOH as the precipitating agent [20,21]. In the general procedure, 2.0 g of the support was added above a solution containing $HAuCl_4{\cdot}3H_2O$ (with the desired gold loading) and stirred at 25 °C for 1 h. Subsequently, a stoichiometric quantity of a 0.1 mol L^{-1} aqueous NaOH solution (OH^-/Au = 3) was added with constant stirring and the system was heated to 100 °C (reflux) until the color changed from yellow to red or purple. The solid product was filtered, washed thoroughly with deionized water until the filtrate contained no chloride ions (confirmed by an $AgNO_3$ test) and subsequently dried in hot air oven at 100 °C for 5 h.

2.3. Characterization

X-ray diffraction (XRD) was performed on a Rigaku X-ray Geigerflex using a Ni filter and Cu Kα radiation at 2–90° in 2Θ range. Infrared spectroscopy (FTIR) was carried out in a Perkin Elmer 1760-X spectrometer using a range of 4000–400 cm^{-1} and KBr pellets. N_2 adsorption-desorption isotherms were recorded at −196 °C in an ASAP 2010 Micromeritics apparatus, the specific surface areas were determined by the BET (Brunauer-Emmett-Teller) equation using the adsorption data over a relative pressure range of 0.05–0.3, and the pore-size distributions were estimated using the Barrett-Joyner-Halenda (BJH) method based on the Kelvin equation [30]. Electrophoresis measurement (EM) was carried out in a Zeta-Meter 3.0+ apparatus using 20 mg of sample suspended in 200 mL of a 1×10^{-3} mol L^{-1} KCl solution. The pH was adjusted with either 0.1 mol L^{-1} HCl or KOH solutions. The IEP (isoelectric point) was obtained from the plot of the pH vs. the zeta potential. UV–vis spectra of diffuse reflectance of solid state was studied in the range of 200–900 nm on a Varian Cary 3 UV–vis spectrophotometer equipped with an area of 150 mm in diameter covered with poly integration tetra-fluoroethylene (PTFE). The dust samples were mounted in a quartz cell, which provided a sample thickness greater than 3 mm and thus guaranteed "infinite" sample thickness. A Philips CM200 model high resolution electron microscope with an energy dispersive analyzer was used for HR-TEM analysis. HR-TEM microscope was provided with a digital camera coupled to a high speed TVIPS FastScan F-114 model with 1024 × 1024 pixels and 12 bits. The samples for analysis were prepared by dispersion in ethanol/H_2O (1:1) and deposited on a holey carbon/Cu grid (300 mesh). Up to 300 individual metal particles were counted for each catalyst, and the surface area-weighted mean Au diameter (d_p) was calculated by the equation:

$$d_p = \frac{\sum_i n_i d_i^3}{\sum_i n_i d_i^2}$$

where n_i is the number of particles of diameter d_i. Chemical analysis was performed by inductively coupled plasma-mass spectrometry on a PerkinElmer 3300 ICP-MS Spectrometer. Samples were solubilized in a nitric/hydrochloric acid solution and homogenized in microwave oven. X-ray photoelectron spectra (XPS) were recorded using an Escalab 200R spectrometer provided with a hemispherical analyzer, operated in a constant pass energy mode and Mg Kα X-ray radiation (h = 1253.6 eV) operated at 10 mA and 12 kV. Charging effects of samples were corrected by fixing the binding energy (BE) of the C1s core-level of adventitious carbon at 284.8 eV (accuracy = ±0.1 eV).

2.4. Catalytic activity measurements in liquid phase

The catalytic assays of the *para*-nitrocompounds ((x)NB) hydrogenation were performed in a stainless steel (100 mL) Parr-type semi-batch reactor at a substrate concentration of 0.02 mol L^{-1} using ethanol (25 mL) as the solvent with stirring at 700 rpm under 40 bar of H_2 pressure. In all cases, (x)NB, where x corresponds to the group in the *para* position (x = H, nitrobenzene; x = Cl, *p*-chloronitrobenzene; x = NO_2, *p*-dinitrobenzene; x = CN, *p*-nitrobenzonitrile; x = CHO, *p*-nitrobenzaldehyde; x = OCH_3, *p*-nitroanisole; x = CH_3, *p*-nitrotoluene; x = OH, *p*-nitrophenol and x = NH_2, *p*-nitroaniline). All of the catalytic runs were conducted under negligible mass transfer resistance as was established using the Madon and Boudart approach [31]. The catalytic runs and analytical quantifications were repeated three times for each experiment. In a blank test, the activity test confirmed the absence of any measurable conversion for a pure MCM-41 and Ti(X)MCM-41. The pseudo-kinetic constants (k) were calculated using a pseudo-first-order kinetic model for a batch reactor under similar conditions, as reported in previous studies [20].

The reactants and products were analyzed by gas chromatography and mass spectrometry using a GC–MS instrument (Shimadzu GCMS-QP5050) with helium as the carrier gas. The recycling assays were performed by filtering the catalyst from the reaction medium. The filtered catalyst was washed three times consecutively with ethanol (50 mL × 3) to clean the surface and was then dried at 100 °C for 24 h (conversion and selectivity were calculated using the equations presented in the supplementary material)

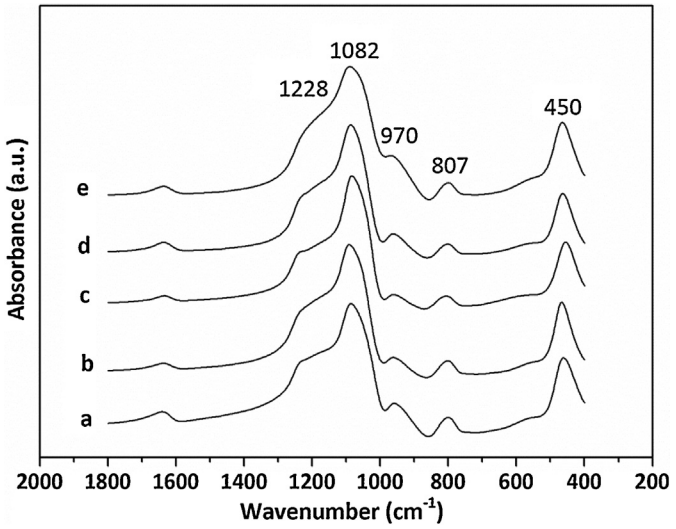

Fig. 1. Infrared spectra for a) Ti(0)-MCM-41, b) Ti(1.0)-MCM-41, c) Ti(2.0)-MCM-41, d) Ti(5.4)-MCM-41 and e) Ti(10.7)-MCM-41.

3. Results and discussion

3.1. Characterization of the supports

The Ti loading of Ti(X)-MCM-41 samples with X ≠ 0 were detected by ICP-MS analysis, and the results are summarized in Table 1. Prepared by the sol-gel method, the real titanium content of Ti(X)-MCM-41 samples corresponded closely to the theoretical value. Table 1 also shows the ZPC values of the Ti(X)-MCM-41 supports. The gradual increase in ZPC with Ti content indicates that the support surface was gradually and homogeneously covered by the Ti species in agreement with the DRUV-Vis and XPS support characterization (*vida infra*).

The presence of a hexagonal phase structured solid in Ti(x)MCM-41 was analyzed by X-ray diffraction (check Supplementary material Fig. S1). The XRD patterns obtained for all of the materials shows the characteristic planes corresponding to the Miller index (*hkl*) corroborating the presence of a hexagonal lattice with symmetry P6 in the synthetized mesoporous solids.

The textural and morphologic properties of the mesoporous molecular sieves modified with different titanium contents were analyzed by N_2 adsorption-desorption isotherms (check Supplementary material Fig. S2). The textural characterization properties of the supports are shown in Table 1. As the content of Ti increases on the Ti(X)-MCM-41 samples S_{BET} diminish [28,32]. This is due to the difference of ionic radios of Si^{4+} (0.041 nm) and Ti^{4+} (0.068 nm) which altered the geometry of the material [15]. The S_{BET} results are in agreement with the XRD supposition involving the segregation to TiO_2 or SiO_2-TiO_2 oxides with different porosity because other diffractions attributed to anatase or rutile crystallographic phases from TiO_2 were not detected.

The FT-IR spectra of Ti(X)-MCM-41 samples are shown in Fig. 1. Two signals are shown at 450 cm^{-1} and 807 cm^{-1}, the first assigned to bending vibration and the second for symmetric stretching vibrations of Si—O—Si bonds. Around 1082 and 1228 cm^{-1} internal and external asymmetric Si—O stretching modes are presented. The band around 970 cm^{-1} can be attributed to two types of signals (i) Si—OH stretching of pure MCM-41 and (ii) Si—O—Ti bonds of the titanium samples [28,33]. These bands have been widely reported and should be interpreted correctly due to the possibility of the overlapping of both Si—OH groups and Ti—O—Si bonds vibrations [34].

Table 2
ICP-MS and metal particle size distribution determined by HR-TEM for Au/MCM-41-Ti(X) catalysts.

Catalyst	Au wt [%]	$d_{HR\text{-}TEM}$ [nm]
Au/Ti(0)-MCM-41	0.28	9.0 ± 3.4
Au/Ti(1.0)-MCM-41	0.62	9.4 ± 2.1
Au/Ti(2.0)-MCM-41	0.80	4.5 ± 2.7
Au/Ti(5.4)-MCM-41	0.96	5.8 ± 2.1
Au/Ti(10.7)MCM-41	0.90	6.0 ± 1.9

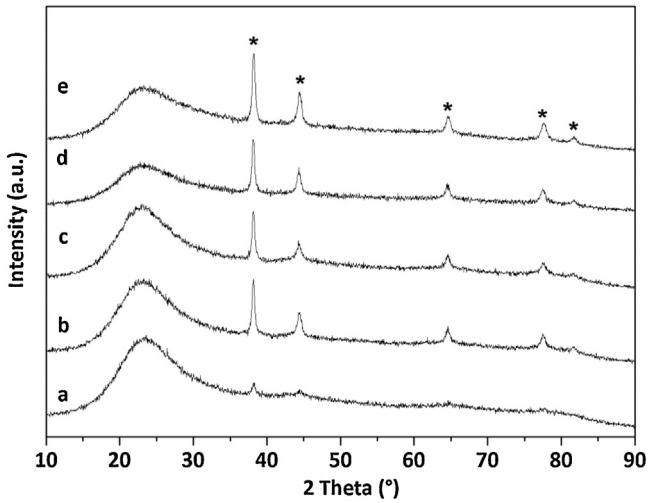

Fig. 2. Diffraction patterns for a) Au/Ti(0)-MCM-41, b) Au/Ti(1.0)-MCM-41, c) Au/Ti(2.0)-MCM-41, d) Au/Ti(5.4)-MCM-41 and e) Au/Ti(10.7)-MCM-41. Reference patterns (*) Au (00-004-0784).

3.2. Catalyst characterization

The real amount of gold deposited on the Ti(X)-MCM-41 was quantified using ICP-MS technique (see Table 2). In the different supports, the amount of gold increased with an increase in the Ti substitution. Using the literature data and our results, we have tried to estimate and identify the possible gold chloro-hydroxy species present as a function of pH during the catalyst synthesis. The supports were in contact with the $AuCl_4^-$ aqueous solution at pH 2.2 for 1 h. After the ion-exchange process, the pH was increased by the addition of NaOH, initiating a sequential hydrolysis to give various hydrolytic products, as mentioned in previous reports [35,36]:

$$AuCl_4^- + xOH^- \rightarrow [Au(OH)_xCl_{4-x}]^- + xCl^-$$

The increase in pH during NaOH addition allows the reaction of the $AuCl_4^-$ precursor and OH- to give a mixed $[AuCl_4^-x(OH)_x]$-species. Thus, a series of ligand substitution reactions between $AuCl_4^-$ and the hydroxide anions occurs, and simultaneously, the Ti(X)-MCM-41 surface is deprotonated, resulting in the formation of anionic species such as M—O^- (where M: Si or Ti). These charged oxygen atoms are basic and allow the substitution of the OH^- groups from the $[AuCl_4^-{}_x(OH)_x]^-$ complex by M—O^- units of the surface support (please check Fig. S3 in Supplementary information). Therefore, the increment in the ZPC of the support with an increase in Ti substitution enhances the deposition of Au nanoparticles via the combined effects of ion-exchange and ligand substitution with the M—O^- surface species.

Catalyst X-ray diffraction is shown in Fig. 2. In all cases, the support structure remains after the deposition of Au NPs. For all catalysts, the reflection lines of Au are clear. In the Au/Ti(0)-MCM-41 catalyst, only the (1 1 1), (2 0 0) and (2 2 0) Miller indices are observed; they are very low intensity and quite wide. This is consistent with the chemical analysis for Au/Ti(0)-MCM-41 that showed

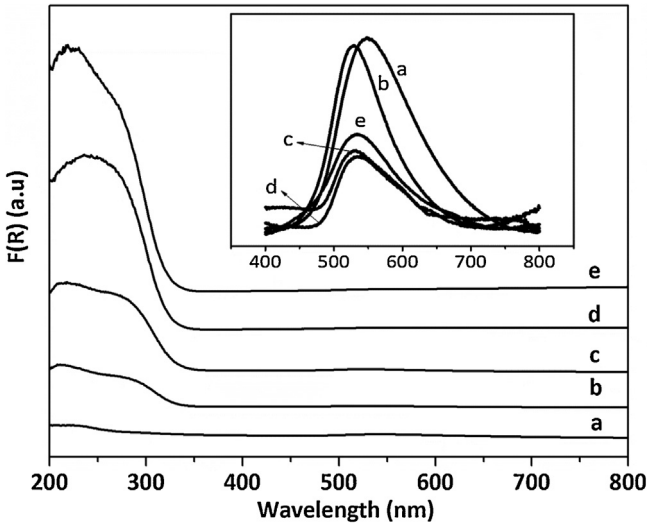

Fig. 3. DRUV–vis spectra of a) Au/Ti(0)-MCM-41, b) Au/Ti(1.0)-MCM-41, c) Au/Ti(2.0)-MCM-41, d) Au/Ti(5.4)-MCM-41 and e) Au/Ti(10.7)-MCM-41.

the lowest amount of gold deposited into the support. The other catalysts in this family exhibit sharp and intense XRD peaks indicative of medium-sized metal Au NPs.

DRUV–vis spectra of the catalysts are shown in Fig. 3. For Au/Ti(X)-MCM-41, an absorption band between 200 and 400 nm is observed. The intensity of the absorption band increased with an increase in the Ti incorporated into the sample. Around 250 nm an intense band is presented characteristic of tetra-coordinated titanium species [28,29]. Extra-framework Ti species have been detected at 238 nm (isolated hexacoordinated Ti) and 200–286 nm (highly dispersed TiO_2 species with particle size < 5.0 nm) [37]. For the samples Au/Ti(1.0)-MCM-41 and Au/Ti(2.0)-MCM-41 we recorded both isolated Ti^{4+} species and a significant quantity of dispersed TiO_2 species with particle size < 5.0 nm. For the other Titanium catalysts (Ti(X)-MCM-41 with X = 5.4 and 10.7) showed mainly dispersed TiO_2 species with particle size <5.0 nm and a low contribution of Ti^{4+} species. The absence of bands in the range 330–340 nm indicates that no separate TiO_2 anatase phase (particle size >5.0 nm) is present in catalyst surface [38]. Therefore, in all of the Ti(X)-MCM-41 samples with X > 0, the UV–vis spectra, N_2 isotherms and XRD conclude that Ti is effectively incorporated in the framework as Ti^{+4} [15,39–42]. The plasmon of Au was observed to be centered at 550 nm [43–45], which indicates that the Au NPs are mostly spherical. The intensity of the plasmon also depends on the particle size [46–49]. Changes in the plasmon intensity of the catalysts were observed; it can be expected that higher particle sizes would be obtained for the catalysts Au/Ti(X)-MCM-41 with X = 0 and 1.0, whereas the catalysts with X = 2.0, 5.4 and 10.7 have similar particle sizes between them, in agreement with the XRD characterization.

The particle size distribution as measured by HR-TEM for the Au/Ti(X)MCM-41 catalysts is shown in Table 2. For Au/Ti(X)MCM-41 catalysts with X: 0 and 1.0, the particle size distribution is broader and larger with an average of 9.0–9.5 nm; however, with an increase in Ti substitution (X > 1.0), the particle size distribution narrows and shifts toward smaller sizes. These results clearly indicate that Ti incorporation decrease gold particles size and improve its dispersion. During the catalysts synthesis, Ti atoms into MCM-41 framework decrease the ZPC of the support surface enhancing the ion-exchange process; besides could be improve the anchorage of the $[AuCl_4^{-}{}_x(OH)_x]^-$ species on Ti—O^- sites. The Au nanoparticles sizes, in all the catalysts, are spherical in agreement with the DRUV–vis results.

The binding energies (BE) determined by XPS are shown in Table 3. The curve fitting of the Au core-level spectrum was performed by using a two spin-orbit split Au $4f_{7/2}$ and Au $4f_{5/2}$. Only the values of level $4f_{7/2}$ of gold were analyzed. In all catalysts, the Au $4f_{7/2}$ photoelectron peak is located at a BE value between 83.7 and 84.1 eV. These values are typical of a pure metallic Au° species [50,51] and confirm that the colloidal procedure allows the metal to be obtained in the zero-valence state. However, it is important to note that Au/Ti(X)-MCM-41 catalysts with X > 1.0 had binding energy values lower than Au/Ti(0)-MCM-41. This might suggest that Au nanoparticles are partially polarized ($Au^{\delta-}$) in the Au/Ti(X)-MCM-41 (X > 1.0) catalysts [20]. The effect of structural arrangements of Au atoms in the surface of nanosized particles on BE must be considered. In all the catalysts mostly spherical Au nanoparticles were detected by DRUV-Vis and TEM. According with results reported by Radnik et al. [52] for small Au nanoparticles low-coordinated surface atoms should dominate the values of $Au4f_{7/2}$ BE. It is well known, that the $Au4f_{7/2}$ electrons of surface atoms have a BE of 83.6 eV attributed to a decrease of the coordination number relative to the bulk metal values ($\Delta BE \sim 0.4$ eV). For this reasons the decrease of the $Au4f_{7/2}$ BE in the Au/Ti(X)-MCM-41 catalysts could be attribute to a decrease of the metal nanoparticles more than the shape of themselves. The atomic ratio of Au/Si suggests an increase in metal dispersion with an increase in Ti loading in the support, in agreement with previous characterizations [20].

Table 3 also shows O1s and Ti2p XPS BE of Ti(X)-MCM-41. For the sample free of Ti, the XPS analysis show one type of oxygen around 532.8 eV, assigned to O1s of Si—O—Si bond [53]. This signal was detected for all of the Ti(X)-MCM-41 samples with different Ti contents because the major contribution from the SiO_2 matrix masks the eventual contribution due to the Si—O—Ti bond [37,54,55]. For Ti containing samples two types of oxygen were detected. The reason of that behaviour is by the titanium distribution on the catalyst surface [56,57]. The Au/Ti(X)-MCM-41 catalysts showed a contribuition at 530.1–530.7 eV that corresponds to the O 1s signal of segregated TiO_2 [37,54]. This contribution could be attributed to two Ti^{4+} components as was discussed in the DRUV-Vis characterization. The Au/Ti(1.0)-MCM-41 and Au/Ti(2.0)-MCM-41 samples showed more homogeneously distributed titanium species because the surface Si/Ti atomic ratios are similar than the bulk values (see Table 3). At higher Ti substitutions, increase the contribution of O1s BE at 530.7 eV could be attributed to Ti species are indeed present as unreacted small TiO_2 particles (not detected by XRD but seen by DRUV–vis) deposited at the external surface region of the supports in agreement with the high Ti/Si atomic ratio.

For the Ti 2p XPS spectra, only the $Ti2p_{3/2}$ was analyzed for the Ti(X)-MCM-41 samples. At a low Ti wt% loading, the spectrum of Ti(1.0)-MCM-41 shows a $Ti2p_{3/2}$ peak at 458.7 eV, which is still approximately 0.4 eV higher than that of TiO_2-anatase. This band is currently associated to the Ti^{4+} present in the solid [58]. Another possibility is attributed the lengthening of the Ti—O bond [59].

4. Catalytic activity

4.1. Hydrogenation of nitrobenzene

The as-prepared catalysts Au/Ti(X)MCM-41 were used to catalyze NB hydrogenation and the results are shown in Fig. 4. All the supported Au catalysts were active in NB hydrogenation and showed pseudo-first-order kinetics with respect to the NB conversion. All catalyst showed good selectivity for aniline (AN) at 25 °C and 40 bar of H_2 pressure. All of the catalysts were chemioselective for NO_2 group hydrogenation and other hydrogenated products such as partial or total phenyl ring hydrogenation, nitroso-, azo- and/or azoxy-derivatives were not detected.

Table 3
Binding energies (eV) of internal electrons and atomic surface ratio of Au/Ti(X)-MCM-41.

Catalyst	Si 2p	Ti $2p_{3/2}$	O 1s	Au $4f_{7/2}$	Au/Si at	Ti/Si (at)	Ti/Si (Bulk)
Au/Ti(0)MCM-41	103.4	–	532.8	84.1	0.0009	–	–
Au/Ti(1.0)MCM-41	103.4	458.6	530.1 (9) 532.9 (91)	84.0	0.0007	0.0150	0.0100
Au/Ti(2.0)MCM-41	103.4	458.7	530.7 (7) 532.9 (93)	83.9	0.0019	0.0280	0.0200
Au/Ti(5.4)MCM-41	103.4	458.7	530.6 (12) 532.9 (88)	83.8	0.0025	0.0680	0.0500
Au/Ti(10.7)MCM-41	103.4	458.9	530.5 (11) 532.9 (89)	83.8	0.0028	0.1340	0.1000

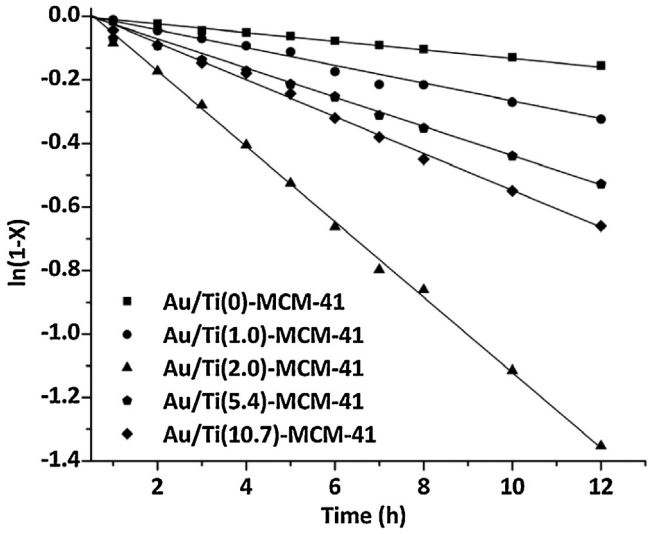

Fig. 4. Conversion data for the hydrogenation of nitrobenzene over Au/Ti(X)-MCM-41 catalysts. Reaction conditions: substrate concentration: 0.02 mol L^{-1}; P_{H2}: 40 bar; catalyst mass: 0.100 g; stirring rate: 700 rpm; solvent: ethanol at 25 °C; reaction time: 12 h.

In Table 4, all of the kinetic constants were normalized using the total amount of Au on the surface to compare the catalytic results according to the different gold metal loading rates on the Au/Ti(X)MCM-41 catalysts (see Table 2). For Au/Ti(2.0)MCM-41, the apparent catalytic rate constant is 2-fold larger than for Au/Ti(0)MCM-41 catalyst. It is worth noting that the Au dispersion ratio for both catalysts $(XPS(Au/Si)_{Au/Ti(2.0)MCM-41}/XPS(Au/Si)_{Au/Ti(0)MCM-41} = 2.1$, Table 3) is similar to the k_g ratio. This suggests that high Au dispersion enhances the NB conversion rate of the Au/Ti(2.0)MCM-41 catalyst. In terms of the AN yield observed for all catalysts, it is apparent that the Ti effect contributes to enhancing the selectivity to AN (Y_{AN}), in agreement with previous reports [21].

Most published papers implement the Haber reaction mechanism [60], which was the only accepted reaction pathway for a long time. Recently, a novel reaction mechanism was proposed by Gelder et al. [61] in which the authors claimed that the Haber mechanism was not adequate. In addition, Turáková et al. published a supplemented reaction mechanism for NB hydrogenation that considers Haber's and Gelder's reaction mechanisms (Scheme 1) [62]. For Au/Ti(X)-MCM-41 catalysts the product analysis during the hydrogenation reaction showed that the selectivity toward phenyl-hydroxylamine was very low (<5.1%) and other intermediate species were not detected. These results are in agreement with a Turákováis reaction mechanism where the hydrogenation reaction avoids the condensation pathways and the production of phenyl-hydroxylamine could be the slow and rate-determining step.

Fig. 5 shows the relationship between the conversion levels at 24 h of reaction and the TOF with the Ti substitution for the different catalysts. A volcano-type tendency was detected, indicating that an optimal amount of Ti exists in the MCM-41 network for this reaction. For the modified supports, Ti incorporation reached a maximum conversion level at 2.0 wt%, which can be explained by both Au loading and Au nanoparticle size. For comparison, Au/Ti(0)MCM-41 showed a poor conversion level and the lowest selectivity for AN. This behavior can be explained by a higher Au nanoparticle size and a low metal loading obtained with this MCM-41 unmodified support.

Table 4
Catalytic data for NB hydrogenation on Au/Ti(X)-MCM-41 catalysts. Reaction conditions: substrate concentration: 0.02 mol L^{-1}; P_{H2}: 40 bar; catalyst mass: 0.100 g; stirring rate: 700 rpm; solvent: ethanol at 25 °C; reaction time: 24 h.

Catalyst	k_g[a] [hg_{Au}^{-1}]	Conversion [%]	TOF[b] [h^{-1}]	Y_{An}[c] [%]
Au/Ti(0)MCM-41	68	27.0	35.7	84.9
Au/Ti(1.0)MCM-41	44	47.6	32.4	95.4
Au/Ti(2.0)MCM-41	129	92.4	43.8	93.1
Au/Ti(5.4)MCM-41	45	65.2	34.1	98.7
Au/Ti(10.7)MCM-41	56	69.8	28.3	98.8

[a] Global reaction pseudo-first-order constant.
[b] at 2 h and surface Au using dispersion calculated from TEM.
[c] Intermediate product: phenyl-hydroxylamine, average values.

Table 5
Catalytic data for NB hydrogenation over Au/Ti(2.0)MCM-41 catalyst using different solvents. Reaction conditions: substrate concentration: 0.02 mol L^{-1}; P_{H2}: 40 bar; catalyst mass: 0.100 g; stirring rate: 700 rpm; temperature: 25 °C; reaction time: 24 h.

Solvent	Dielectric Constant[a]	Conversion [%]	Yield An[b] [%]	TOF[c] [h^{-1}]	k_g[d] [$h^{-}g_{cat}^{-1}$]
Methanol	33	95.9	81.5	58.7	1.34
Ethanol	24	92.5	94.9	43.8	1.08
Isopropanol	18	61.2	99.8	24.3	0.40
Tetrahydrofuran	7.0	14.2	100.0	3.8	0.06
Toluene	2.4	65.2	99.9	23.1	0.44
Cyclohexane	2.0	43.8	97.6	14.8	0.23

[a] Data from Ref. [61].
[b] Average values.
[c] 2 h of reaction.
[d] Global reaction pseudo-first-order constant.

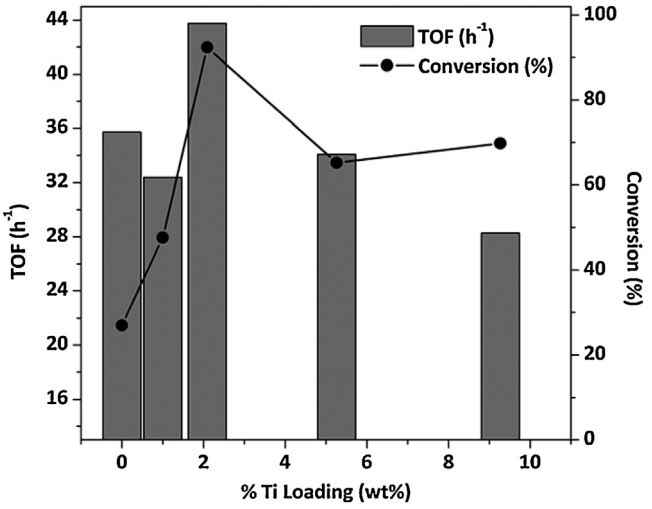

Fig. 5. Conversion and TOF for the hydrogenation of NB on Au/Ti(X)-MCM-41 catalysts at different Titanium contents. Reaction conditions: substrate concentration: 0.02 mol L^{-1}; P_{H2}: 40 bar; catalyst mass: 0.100 g; stirring rate: 700 rpm; solvent: ethanol at 25 °C; reaction time: 24 h.

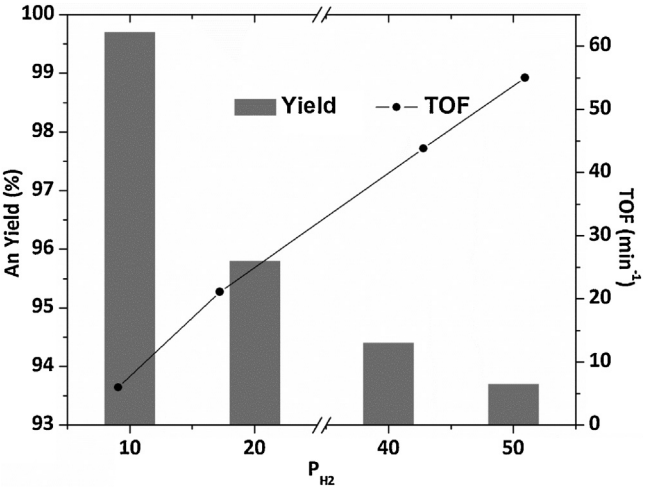

Fig. 6. Yield of aniline and TOF for the hydrogenation of nitrobenzene on Au/Ti(2.0)-MCM-41 catalyst at different H_2 pressures. Reaction conditions: substrate concentration: 0.02 mol L^{-1}; P_{H2}: 40 bar; catalyst mass: 0.100 g; stirring rate: 700 rpm; solvent: ethanol at 25 °C.

4.2. Effect of H_2 pressure

After finding the most selective catalytic system, i.e., Au/Ti(2.0)MCM-41, the effect of the hydrogen pressure was studied. Fig. 6 shows both TOF and AN yield as a function of the H_2 pressure. The surface H_2 concentration might directly influence the reactant adsorption and modify the catalytic activity. An increase in H_2 pressure (from 10 to 50 bar) markedly affects the TOF but only slightly alters the yield. The approximately linear plot of TOF values versus hydrogen pressure indicates first-order kinetics with respect to hydrogen pressure. In all of the pressure ranges studied, a slight increase in undesirable intermediate products, mainly phenyl-hydroxylamine, was detected at elevated pressure. It can be concluded that an increase in the H_2 pressure could promote an incomplete $-NO_2$ group hydrogenation by competitive hydrogen adsorption. At a higher H_2 pressure, the production of AN from phenyl-hydroxylamine hydrogenation could be the rate-determining step, which increased the phenyl-hydroxylamine concentration, even at the maximum conversion level (see Table S1).

Table 6
ICP and XPS data for the recyclability of the Au/Ti(2.0)MCM-41 catalyst. Reaction conditions: 0.02 mol L^{-1}, P_{H2}: 40 bar, catalyst mass: 0.100 g, stirring rate: 700 rpm, solvent: ethanol at 25 °C.

Cycle	Au wt[%]	Au $4f_{7/2}$ (eV)	Au/Si at	Ti/Si at
First	0.80	83.9	0.0019	0.0280
Final	0.10	traces	–	0.0264

4.3. Effect of the solvent

The effect of solvents with dielectric constants ranging from 2 to 33 (the values are for pure solvents [63]) have been included in this study for the hydrogenation of NB catalyzed by Au/Ti(2.0)MCM-41, and the results are displayed in Table 5. From these results, it is clear that the Au/Ti(2.0)MCM-41 conversion for NB hydrogenation was strongly influenced by the solvent employed to carry out the reaction. The activity pattern with the protic solvents was: methanol > ethanol > 2-propanol. If aprotic solvents are considered, the activity followed the pattern: toluene > cyclohexane ≫ tetrahydrofuran. Amazingly, a very low NB conversion was observed when tetrahydrofuran was used as the solvent. Kinetic results showed a satisfactory correlation between catalyst activity for NB hydrogenation and solvent polarity was verified only for protic alcohol solvents; the kinetic constant increases as the corresponding polarity parameter increases. This is in agreement with the studies of Rojas et al. for the citral hydrogenation [64] and Bertero et al. in the heterogeneous hydrogenation of acetophenone [65].

On the contrary the yield to aniline was affected by the polarity of the alcohols chosen. Many reports indicates that the solvent not only affect the kinetics but also the H_2 solubility, adsorption of reactant into the active site, among others [66]. Particularly for this reaction, solvation of the reactant could be the main problem due to high intermolecular forces (dipole–dipole and H-bond) between the substrate and solvent. The formation of a solvation complex is enhanced in small and high polarity solvents. This effect can block an optimal adsorption in the active site of the catalyst and promote a decrease of aniline production. Explaining why the hydrogenation yield diminishes as C atoms in the alcohol decrease.

For aprotic solvent no clear relationship was found for activity or yield parameters in correlation with solvent polarity or dielectric constant. However, with tetrahydrofuran as the solvent, the NB hydrogenation rate is lower for the aprotic apolar solvent. This is because the solvent–NB interaction is stronger for aprotic polar than for polar solvents (cyclohexane and toluene), which increases the competing solvation at the active site, consequently hindering the NB adsorption on the catalyst surface. The adsorption of tetrahydrofuran on the surface of Au atoms might partially block the active site for NB adsorption, thereby decreasing the catalyst activity as detected in similar Pt/TiO_2 catalytic systems [67].

4.4. Catalyst recycling

Catalyst recycling tests were carried out in the same apparatus. After each reaction cycle, the catalyst was washed with ethanol to remove organic matter that could have been adsorbed on the support and the reaction mixture was filled with new NB. Representative activity data are shown in Fig. 7. After the first run, a significant drop in catalyst activity was observed. The catalysts showed an obvious decay of catalytic performance in the second reaction cycle due to serious leaching of the Au content as shown in Table 6. The leaching problem in this study was confirmed by XPS

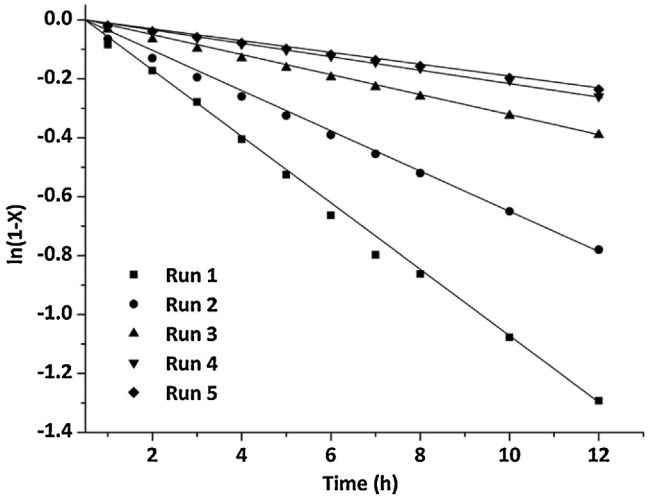

Fig. 7. Evolution of conversion in function of the run for hydrogenation of nitrobenzene over Au/Ti(2.0)-MCM-41 catalysts. Reaction conditions: substrate concentration: 0.02 mol L^{-1}; P_{H2}: 40 bar; catalyst mass: 0.100 g; stirring rate: 700 rpm; solvent: ethanol at 25 °C; reaction time: 12 h.

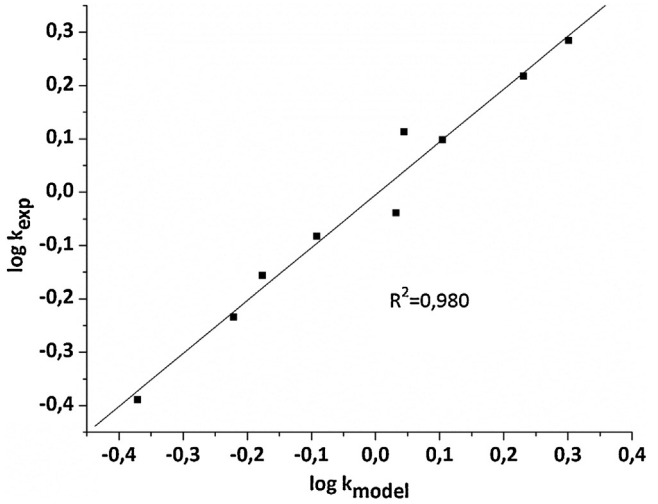

Fig. 8. Correlation between log k_{exp} and log k_{model} for *para*-substituted nitrobenzene hydrogenation on Au/Ti(2.0)MCM-41 catalyst. Conditions: a batch reactor, T = 25 °C, 40 bar of H_2 pressure, 0.02 mol L^{-1} nitrocompound concentration.

characterization. Before the reaction, the Au nanoparticles were well dispersed in the Ti(2.0)MCM-41 support as discussed in the characterization section. After the fifth reaction cycle, a low Au wt% content was detected by ICP analysis, in agreement with a trace of Au atoms on the catalyst surface shown by XPS measurement. This indicates that the major part of the Au nanoparticles leached out during the cycles. In addition, a constant value of the Ti/Si surface atomic ratio after the last cycle was observed, which could be attributed to the non-leaching of the Ti species during the cycles.

4.5. para-*Substituted nitrobenzene hydrogenation and quantitative multilinear correlation*

At this stage, we analyzed the hydrogenation reaction of different nitrobenzene compounds substituted in the – *para* position that had different substituents, electron-withdrawing or – donating groups. The catalytic activity is dependent on the substituent group in the *para* position; an electron-withdrawing or – donating substituent differs in its ability to withdraw or supply electrons from or to the reaction site. The effect of the *para*-substituent on the catalytic activity is shown in Table 7. For electron-withdrawing substituents, the hydrogenation reaction is activated, reaching a higher activity than the NB hydrogenation because of the poor stabilization of the $-NO_2$ group, which increases the reduction velocity for $-NH_2$ products. The following activity sequence was established for electron-withdrawing groups: p-(NO_2)NB > p-(CN)NB > p-(Cl)NB > p-(CHO)NB > NB. Pseudo-first-order kinetics with respect to the reactant was found for all of the substrates. For electron-donating substituents, the catalytic activity was lower than the NB due to the stabilization of the resonance and inductive effects on the $-NO_2$ group. It was observed that p-(CH_3)NB, p-(OCH_3)NB, p-(OH)NB and p-(NH_2)NB derivatives had low initial rates, which could indicate that strong donor groups deactivate the $-NO_2$ group, making the reaction difficult to initiate.

The selectivity of the reaction for the desired product (aniline derivative) was maximum for all substituted nitrobenzene substrates analyzed. This indicates that the reaction favors the formation of the aromatic amine. Intermediates were detected in trace concentrations, and the reaction therefore provides a more direct pathway to the $-NO_2$ group reduction.

To establish a quantitative relationship between the catalytic activity and substituent effects, a multilinear relationship model was developed. In our multiple linear regression model, the electronic effect (σ_{para}) and the hydrophobicity parameter (π) for each substituent group were used. The Hammett constant (σ) is an empirical descriptor that characterizes the electronic effects associated with various functional groups. The hydrophobicity constant (π) is an empirical descriptor associated with the hydrophobicity of a substituent group. Thus, a value of $\pi > 0$ indicates a hydrophobic group and $\pi < 0$ indicates a hydrophilic group (see Table 7). The correlations between these two structural parameters and the observed catalytic activity of *p*-substituted nitrobenzenes lead to the following equation:

$$log k_{mod} = -0.03867 + 0.4328\sigma_{para} + 0.0525\pi$$

This equation indicates that the electronic substituent effects (0.4328σ) are more important than the hydrophobicity effects (0.0525π), which is in good agreement with the Hammett analysis of the mechanism proposed for this type of reaction [68,69]. Fig. 8 shows the high confidence level (99%) of the model with respect to experimental data. The correlation coefficient for σ values could be used as an estimation of the charge development during the course of the reaction and provides a measure of the susceptibility of the system to substituent electronic effects. In a nucleophilic attack, the reaction rate is enhanced by electron-withdrawing substituents and $\sigma_\sigma > 0$, while σ_σ values close to 0 are indicative of a partially charged transition state. The value of a_σ is positive (0.4328), which explains that this type of reaction could proceed via a nucleophilic mechanism and indicates a greater dependence of the rate on the electronic character of the substituent than on the hydrophobic character of the substituent.

5. Conclusions

Ti(X)MCM-41-type molecular mesoporous with different compositions have been successfully prepared by hydrothermal synthesis. The insertion of titanium onto the silica framework was mainly in tetrahedral isolated sites, which was confirmed by DRUV–vis and XPS. A structural characterization established that Ti substitution strongly affected the nucleation and growth of Au nanoparticles and led to quite a large difference in the metal particle size. The Au/Ti(X)MCM-41 catalysts were active in the hydrogenation of nitrobenzene in the liquid phase and promoted the chemoselective reduction of the $-NO_2$ group and showed pseudo-first-order kinetics with respect to the reactant in all cases. Different

Table 7
Catalytic data for *para*-substituited substrates hydrogenation over 1%Au/Ti(2.0)-MCM-41 catalyst. Reaction conditions: Substrate concentration: 0.02 mol L^{-1}, P_{H2}: 40 bar, catalyst mass: 0.100 g, stirring rate: 700 rpm, solvent: ethanol at 25 °C, reaction time: 7 h.

Substrate	Conversion [%]	$Yield_{An}$[a] [%]	TOF[b] [h^{-1}]	k_g[c] [h^{-1} $g_{cat}{}^{-1}$]	k_{model}	σ	π
NB	55.0	94.4	44.3	1.08	0.92	0.00	0.00
p-NBCl	57.9	98.7	52.1	1.27	1.25	0.23	0.71
p-NBCHO	53.1	99.1	61.3	1.10	1.30	0.43	−0.65
p-$NBNO_2$	77.1	95.1	85.4	2.00	1.92	0.78	−0.28
p-NBCN	70.0	100	88.6	1.70	1.65	0.66	0.57
p-$NBNH_2$	30.5	95.6	12.0	0.43	0.41	−0.66	−1.23
p-$NBOCH_3$	41.9	90.0	15.3	0.67	0.70	−0.27	−0.02
p-$NBCH_3$	52.8	98.3	34.2	0.81	0.83	−0.17	0.56
p-NBOH	32.3	85.4	20.5	0.60	0.58	−0.37	−0.67

[a] Average values.
[b] 2 h of reaction.
[c] Global reaction pseudo-first-order constant.

Ti loading systems showed different catalytic activity and selectivity. The catalytic activity increased slightly for the hydrogenation of NB as the Au nanoparticles decreased. The best catalytic system was Au/Ti(2.0)MCM-41, which had pseudo-first-order reaction kinetics with respect to NB and pseudo-first-order kinetics with respect to H_2. The solvent effect studies showed a non-linear correlation between the nature of the solvent and the activity. The most active catalyst showed poor reusability under optimum conditions, and a decrease in the conversion levels was attributed to the leaching of gold nanoparticles during the runs.Finally, for the hydrogenation of *para*-substituted nitrobenzene derivatives, the reaction kinetics depend on the type of substituent, and a quantitative multilinear relationship was determined. The incorporation of two parameters (σ Hammett value and π hydrophobicity parameter) indicates that the electronic effects are the predominant factor and that the hydrogenation reaction over this catalyst occurs by a nucleophilic mechanism.

Acknowledgements

The authors thank the Project FONDECYT 1100259 and 1130005, FONDECYT Postdoctoral 3140157 and FONDECYT Postdoctoral 3140130 and Red Doctoral REDOC, MINEDUC project UCO1202.

Appendix A. Supplementary data

Supplementary data associated with this article can be found, in the online version, at http://dx.doi.org/10.1016/j.apcata.2016.02.013.

References

[1] J.M. Thomas, Angew. Chem. Int. Ed. Engl. 33 (1994) 913–937.
[2] R.A.A. Melo, M.V. Giottoa, J. Rochab, E.A. Urquieta-Gonzáleza, Mater. Res. 2 (1999) 173–179.
[3] C.T. Kresge, M.E. Leonowicz, W.J. Roth, J.C. Vartuli, J.S. Beck, Nature 359 (1992) 710–712.
[4] J.C. Vartuli, K.D. Schmitt, C.T. Kresge, W.J. Roth, M.E. Leonowicz, S.B. McCullen, S.D. Hellring, J.S. Beck, J.L. Schlenker, Chem. Mater. 6 (1994) 2317–2326.
[5] N. Marín-Astorga, G. Pecchi, J.L. García-Fierro, P. Reyes, Catal. Lett. 91 (2003) 115.
[6] A. Corma, Chem. Rev. 97 (1997) 2373–2419.
[7] M.P. Davis, D. Walsh, S.B. Legrand, R. Lagman, J. Palliat. Med. 5 (2002) 813–814.
[8] A. Ortlam, J. Rathouský, G. Schulz-Ekloff, A. Zukal, Microporous Mater. 6 (1996) 171–180.
[9] A. Taguchi, F. Schüth, Microporous Mesoporous Mater. 77 (2005) 1–45.
[10] S. Basu, M. Mapa, C.S. Gopinath, M. Doble, S. Bhaduri, G.K. Lahiri, J. Catal. 239 (2006) 154–161.
[11] V.R. Choudhary, R. Jha, Microporous Mesoporous Mater. 119 (2009) 360–362.
[12] H. Liu, G. Lu, Y. Guo, Y. Wang, Y. Guo, J. Colloid Interface Sci. 346 (2010) 486–493.
[13] N. Maity, S. Basu, M. Mapa, P.R. Rajamohanan, S. Ganapathy, C.S. Gopinath, S. Bhaduri, G.K. Lahiri, J. Catal. 242 (2006) 332–339.
[14] M. Sui, J. Liu, L. Sheng, Appl. Catal. B 106 (2011) 195–203.
[15] S. Wang, Y. Shi, X. Ma, Microporous Mesoporous Mater. 156 (2012) 22–28.
[16] N. Yao, C. Pinckney, S. Lim, C. Pak, G.L. Haller, Microporous Mesoporous Mater. 44–45 (2001) 377–384.
[17] A. Kumar, V.P. Kumar, V. Vishwanathan, K.V.R. Chary, Mater. Res. Bull. 61 (2015) 105–112.
[18] P.R. Selvakannan, K. Mantri, J. Tardio, S.K. Bhargava, J. Colloid Interface Sci. 394 (2013) 475–484.
[19] C. Campos, C. Torres, M. Oportus, M.A. Peña, J.L.G. Fierro, P. Reyes, Catal. Today 213 (2013) 93–100.
[20] C.H. Campos, M. Jofré, C.C. Torres, B. Pawelec, J.L.G. Fierro, P. Reyes, Appl. Catal. A 482 (2014) 127–136.
[21] C. Torres, C. Campos, J.L.G. Fierro, M. Oportus, P. Reyes, Catal. Lett. 143 (2013) 763–771.
[22] H.-U. Blaser, H. Steiner, M. Studer, ChemCatChem 1 (2009) 210–221.
[23] R.A.W. Johnstone, A.H. Wilby, I.D. Entwistle, Chem. Rev. 85 (1985) 129–170.
[24] B. Chen, F. Li, Z. Huang, T. Lu, G. Yuan, Appl. Catal. A 481 (2014) 54–63.
[25] X. Zhang, Y.C. Guo, Z. Cheng Zhang, J.S. Gao, C.M. Xu, J. Catal. 292 (2012) 213–226.
[26] T. Joseph, K. Vijay Kumar, A.V. Ramaswamy, S.B. Halligudi, Catal. Commun. 8 (2007) 629–634.
[27] J.S. Beck, J.C. Vartuli, W.J. Roth, M.E. Leonowicz, C.T. Kresge, K.D. Schmitt, C.T.-W. Chu, D.H. Olson, E.W. Sheppard, S.B. McCullen, J.B. Higgins, J.L. Schlenkert, J. Am. Chem. Soc. 114 (1992) 10834.
[28] G.A. Eimer, S.G. Casuscelli, G.E. Ghione, M.E. Crivello, E.R. Herrero, Appl. Catal. A 298 (2006) 232–242.
[29] G.A. Eimer, C.M. Chanquia, K. Sapag, E.R. Herrero, Microporous Mesoporous Mater. 116 (2008) 670–676.
[30] E.P. Barrett, L.G. Joyner, P.P. Halenda, J. Am. Chem. Soc. 73 (1951) 373–380.
[31] M. Boudart, Adv. Catal. 20 (1969) 153–166.
[32] K. Murata, Y. Liu, M. Inaba, N. Mimura, Catal. Today 91-92 (2004) 39–42.
[33] N.N. Opembe, E. Vunain, A.K. Mishra, K. Jalama, R. Meijboom, J. Therm. Anal. Calorim. 117 (2014) 701–710.
[34] M. Guidotti, N. Ravasio, R. Psaro, G. Ferraris, G. Moretti, J. Catal. 214 (2003) 242–250.
[35] S. Ivanova, C. Petit, V. Pitchon, Appl. Catal. A 267 (2004) 191–201.
[36] P.J. Murphy, M.S. LaGrange, Geochim. Cosmochim. Acta 62 (1998) 3515–3526.
[37] G. Moretti, A.M. Salvi, M.R. Guascito, F. Langerame, Surf. Interface Anal. 36 (2004) 1402–1412.
[38] M.V. Cagnoli, S.G. Casuscelli, A.M. Alvarez, J.F. Bengoa, N.G. Gallegos, N.M. Samaniego, M.E. Crivello, G.E. Ghione, C.F. Pérez, E.R. Herrero, S.G. Marchetti, Appl. Catal. A 287 (2005) 227–235.
[39] J.A. Melero, J.M. Arsuaga, P.D. Frutos, J. Iglesias, J. Sainz, S. Blázquez, Microporous Mesoporous Mater. 86 (2005) 364–373.
[40] S. Bordiga, S. Coluccia, C. Lamberti, L. Marchese, A. Zecchina, F. Boscherini, F. Buffa, F. Genoni, G. Leofanti, J. Phys. Chem. 98 (1994) 4125–4132.
[41] D. Trong On, M.P. Kapoor, P.N. Joshi, L. Bonneviot, S. Kaliaguine, Catal. Lett. 44 (1997) 171–176.
[42] D. Trong On, S.V. Nguyen, V. Hulea, E. Dumitriu, S. Kaliaguine, Microporous Mesoporous Mater. 57 (2003) 169–180.
[43] C.F. Bohren, D.R. Huffman, Absorption and Scattering of Light by Small Particles, John Wiley, New York, 1983.
[44] M. Kerker, The Scattering of Light and Other Electromagnetic Radiation, Academic Press, New York, 1969.
[45] R. Fenger, E. Fertitta, H. Kirmse, A.F. Thunemann, K. Rademann, Phys. Chem. Chem. Phys. 14 (2012) 9343–9349.
[46] C.A. Mirkin, R.L. Letsinger, R.C. Mucic, J.J. Storhoff, Nature 382 (1996).
[47] H.K.M. Tanaka, M. McIntire, R. Castillo-Garza, Microporous Mesoporous Mater. 85 (2005) 374–380.
[48] A. Taleb, C. Petit, M.P. Pileni, Chem. Mater. 9 (1997) 950–959.
[49] A. Henglein, J. Phys. Chem. 97 (1993) 5457–5471.
[50] M.P. Casaletto, A. Longo, A. Martorana, A. Prestianni, A.M. Venezia, Surf. Interface Anal. 38 (2006) 215–218.
[51] A.M. Visco, F. Neri, G. Neri, A. Donato, C. Milone, S. Galvagno, Phys. Chem. Chem. Phys. 1 (1999) 2869–2873.
[52] J. Radnik, C. Mohr, P. Claus, Phys. Chem. Chem. Phys. 5 (2003) 172–177.

[53] T.L. Barr, Zeolites 10 (1990) 760–765.
[54] B.J. Aronson, C.F. Blanford, A. Stein, Chem. Mater. 9 (1997) 2842–2851.
[55] D.P. Wang, H.C. Zeng, Chem. Mater. 21 (2009) 4811–4823.
[56] M.-Y. Kim, S. Jung, M. Kim, Y. You, J.-H. Park, C.-H. Shin, G. Seo, Catal. Lett. 129 (2009) 194–206.
[57] L. Zhang, Y. Zhao, H. Dai, H. He, C.T. Au, Catal. Today 131 (2008) 42–54.
[58] V.-H. Nguyen, S.D. Lin, J.C.S. Wu, H. Bai, Catal. Today 245 (2015) 186–191.
[59] Z. Luan, E.M. Maes, P.A.W. van der Heide, D. Zhao, R.S. Czernuszewicz, L. Kevan, Chem. Mater. 11 (1999) 3680–3686.
[60] F. Haber, Z. Elektrochem. 4 (1898) 506–513.
[61] E.A. Gelder, S.D. Jackson, C.M. Lok, Chem. Comm. (2005) 522–524.
[62] M. Turáková, T. Salmi, K. Eränen, J. Wärnå, D.Y. Murzin, M. Králik, Appl. Catal. A 499 (2015) 66–76.
[63] C.H. Campos, C. Torres, J.L.G. Fierro, P. Reyes, Appl. Catal. A 466 (2013) 198–207.
[64] H. Rojas, J.L.G. Fierro, P. Reyes, J. Chile Chem. Soc. 52 (2007) 1155–1159.
[65] N.M. Bertero, A.F. Trasarti, C.R. Apesteguía, A.J. Marchi, Appl. Catal. A 394 (2011) 228–238.
[66] U.K. Singh, M.A. Vannice, Appl. Catal. A 255 (2003) 361.
[67] C.H. Campos, C.C. Torres, A.B. Dongil, D. Ruiz, J.L.G. Fierro, P. Reyes, Catal. Today 235 (2014) 226–236.
[68] F. Cárdenas-Lizana, Z.M.D. Pedro, S. Gómez-Quero, M.A. Keane, J. Mol. Catal. A 326 (2010) 48–54.
[69] F. Cárdenas-Lizana, D. Lamey, S. Gómez-Quero, N. Perret, L. Kiwi-Minsker, M.A. Keane, Catal. Today 173 (2011) 53–61.